Supplement of Atmos. Chem. Phys., 20, 10193–10210, 2020
https://doi.org/10.5194/acp-20-10193-2020-supplement

Atmospheric Chemistry and Physics
Open Access
EGU

Supplement of

Characterization and source apportionment of aerosol light scattering in a typical polluted city in the Yangtze River Delta, China

Dong Chen et al.

Correspondence to: Yu Zhao (yuzhao@nju.edu.cn)

Number of tables: 5 **Number of figures: 15**

Table list

Figure list

Figure S8. Linear regressions between the measured daily scattering coefficients and those calculated with the IMPROVE1999 algorithm (a) and the IMPROVE2007 algorithm (b) at the three sites.

Figure S9. Linear regressions between the mass scattering efficiencies (MSE) of NH_4NO_3 (a) and $(NH_4)_2SO_4$ (b) estimated with the Mie theory and those with the two version of US IMPROVE algorithms.

Figure S10 The collective proportions of sea salt and soil dust to the total $PM_{2.5}$ scattering coefficient at the three sites

Figure S11. Hygroscopic growth curve of $PM_{2.5}$ at NJU.

Figure S12. The correlation between the scattering coefficients estimated by f(RH) and those simulated with Mie theory under the ambient conditions.

Figure S13. The comparison of the observed scattering coefficients and those estimated with the external, internal, core-shell mixture assumption under the ambient condition at NJU.

Figure S14. The box plots of the ratios of light absorption BrC mass to the total BrC mass under the three pollution levels. The box plots indicate the mean concentration (square symbols) and the maximum, 99th, 75th, 50th, 25th, 1st percentiles, and minimum.

Figure S15. The source profiles for accumulation mode particles from the PMF model at NJU (a), PAES (b) and NUIST (c).

S1. IMPROVE1999 and IMPROVE2007 algorithms

The $PM_{2.5}$ scattering coefficient could be calculated with two IMPROVE algorithms, as described in Pitchford et al. (2007). Briefly, the IMPROVE1999 and IMPROVE2007 algorithms are expressed with Eqs. (S1) and (S2), respectively:

$$b_{sca} \approx 3\times f(RH)[Sulfate] + 3\times f(RH)[Nitrate] + 4\times[Organic\ Mass] + 1\times[Fine\ soil] \quad \text{(S1)}$$

$$\begin{aligned} b_{sca} \approx\ & 2.2\times f_s(RH)[Small\ Sulfate] + 4.8\times f_L(RH)[Large\ Sulfate] \\ & + 2.4\times f_s(RH)[Small\ Nitrate] + 5.1\times f_L(RH)[Large\ Nitrate] \\ & + 2.8\times[Small\ Organic\ Mass] + 6.1\times[Large\ Organic\ Mass] \\ & + 1\times[Fine\ soil] + 1.7\times f_{SS}(RH)[Sea\ salt] \end{aligned} \quad \text{(S2)}$$

The four major components in Eq. (S1) are sulfate (assumed to be $(NH_4)_2SO_4$), nitrate (assumed to be NH_4NO_3), organic mass (assumed to be organic compounds), and fine soil (crustal elements plus oxides). The $PM_{2.5}$ scattering coefficient can be thus estimated by multiplying the concentrations of the four chemical components by typical component-specific mass scattering efficiencies. *f(RH)* denotes the water growth terms for sulfate and nitrate.

IMPROVE2007 separates the large and small particle modes for sulfate, nitrate and OM using a simple mixing model, and different mass scattering efficiencies are used for the two modes (Eq. (S2)). With an assumption of log-normal mass size distribution, the large and small modes are described by the D_g and geometric standard deviations (σ_g) at 0.5 μm and 1.5, and 0.2 μm and 2.2, respectively. Empirically, the fraction of each particle component in the large mode can be calculated by dividing the total concentration of the component by 20 $\mu g/m^3$. If the concentration is above 20 $\mu g/m^3$, all the mass is considered to be in the large mode. A sea salt term is added as a particular concern for coastal monitoring sites. The water growth curves for sea salt and the large and small particle modes of sulfate and nitrate can be referred to Pitchford et al. (2007).

Tables

Table S1. The hygroscopic growth factors (GF) of particles at different particle sizes and RH levels in Nanjing from previous studies (Li et al., 2015; Wu, 2014; Xu et al., 2015; Yu et al., 2015; Zhang et al., 2011).

RH(%)	80 nm	130 nm	200 nm	398 nm
50	1.03	1.03	1.04	1.04
60	1.03	1.05	1.04	1.04
73	1.12	1.14	1.14	1.11
77	1.17	1.19	1.18	1.12
82	1.25	1.28	1.28	1.23
85	1.28	1.34	1.35	1.28
88	1.31	1.41	1.39	1.31
90	1.41	1.45	1.49	1.27

Table S2. The source apportionment of the primary and secondary aerosols for accumulation mode particles at NJU (Unit: %).

Source	Primary apportionment by PMF	Secondary aerosol allocation					Total
		Sector category	Proportions of SO_2 and NO_2 emissions	Proportion of SIA	Proportion of VOCs	Proportion of SOA	
Coal combustion	21.5	Power plants	41.5	10.9			32.3
Industrial pollution	5.1	Chemical industry	13.0	3.4	49.0	1.5	16.8
		Steel industry	13.0	3.4	10.0	0.3	
		Cement industry	7.0	1.8	-		
		Coating industry	-		11.0	0.3	
		Other industrial solvent	-		5.0	0.2	
		Other industries	3.0	0.8	-		
Vehicle	21.0	On road vehicle	12.0	3.1	10.0	0.3	24.4
Fugitive dust	18.4	-	-		-		18.4
Biomass burning	4.9	-	0.7	0.2	1.4	0.0	5.1
Others		-	9.8	2.6	13.6	0.4	3.0
Total	70.8	-	100.0	26.2	100.0	3.0	100.0

Table S3. The same as Table S2 but for PAES.

Source	Primary apportionment by PMF	Secondary aerosol allocation					Total
		Sector category	Proportions of SO_2 and NO_2 emissions	Proportion of SIA	Proportion of VOCs	Proportion of SOA	
Coal combustion	21.9	Power plants	41.5	11.0			32.9
Industrial pollution	2.3	Chemical industry	13.0	3.4	49.0	1.0	13.3
		Steel industry	13.0	3.4	10.0	0.2	
		Cement industry	7.0	1.8	-	-	
		Coating industry	-	-	11.0	0.2	
		Other industrial solvent	-	-	5.0	0.1	
		Other industries	3.0	0.8	-	-	
Vehicle	27.1	On road vehicle	12.0	3.2	10.0	0.2	30.4
Fugitive dust	11.5	-	-	-	-	-	11.5
Biomass burning	6.2	-	0.7	0.2	1.4	0.0	6.4
Others	2.6	-	9.8	2.6	13.6	0.3	5.4
Total	71.6	-	100.0	26.4	100.0	2.0	100.0

Table S4. The same as Table S2 but for NUIST.

Source	Primary apportionment by PMF	Secondary aerosol allocation					Total
		Sector category	Proportions of SO_2 and NO_2 emissions	Proportion of SIA	Proportion of VOCs	Proportion of SOA	
Coal combustion	22.4	Power plants	41.5	10.0			32.4
Industrial pollution	9.6	Chemical industry	13.0	3.1	49.0	2.9	22.8
		Steel industry	13.0	3.1	10.0	0.6	
		Cement industry	7.0	1.7	-	-	
		Coating industry	-	-	11.0	0.7	
		Other industrial solvent	-	-	5.0	0.3	
		Other industries	3.0	0.7	-	-	
Vehicle	21.0	On road vehicle	12.0	2.9	10.0	0.6	24.5
Fugitive dust	13.0	-	-	-	-	-	13.0
Biomass burning	3.9	-	0.7	0.2	1.4	0.1	4.1
Others		-	9.8	2.4	13.6	0.8	3.2
Total	69.9	-	100.0	24.1	100.0	6.0	100.0

Table S5. The contributions of chemical components to the light scattering for accumulation mode particles based on the Mie theory (Unit: %).

Locations	$(NH_4)_2SO_4$	NH_4NO_3	OM	others
NJU	24.3	25.5	31.0	16.6
PAES	21.3	23.6	29.4	23.1
NUIST	25.8	18.7	32.9	20.4

Figures

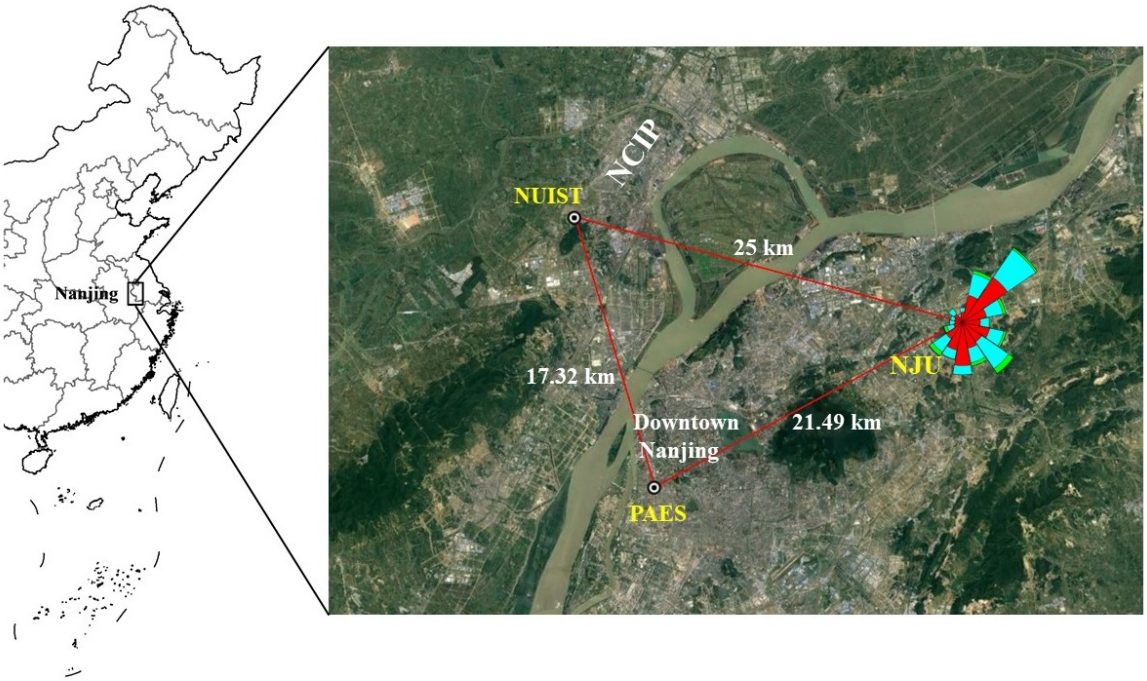

Figure S1. The locations of NJU, PAES and NUIST sites in Nanjing. The map data provided by © Google (Google Earth) are freely available for academic use (http://www.google.cn/intl/zh-CN/earth/).

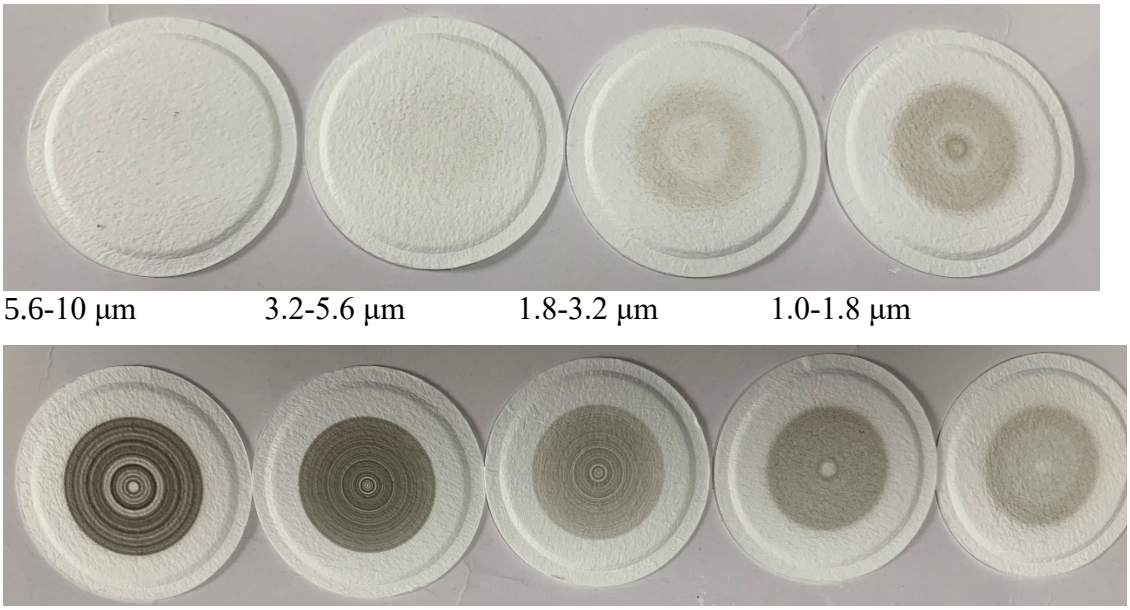

Figure S2. A set of size-resolved particle filter samples on 25 Dec 2015 at NJU. The measured PM1.8 and PM2.5 were 128 and 141μg/m3, respectively.

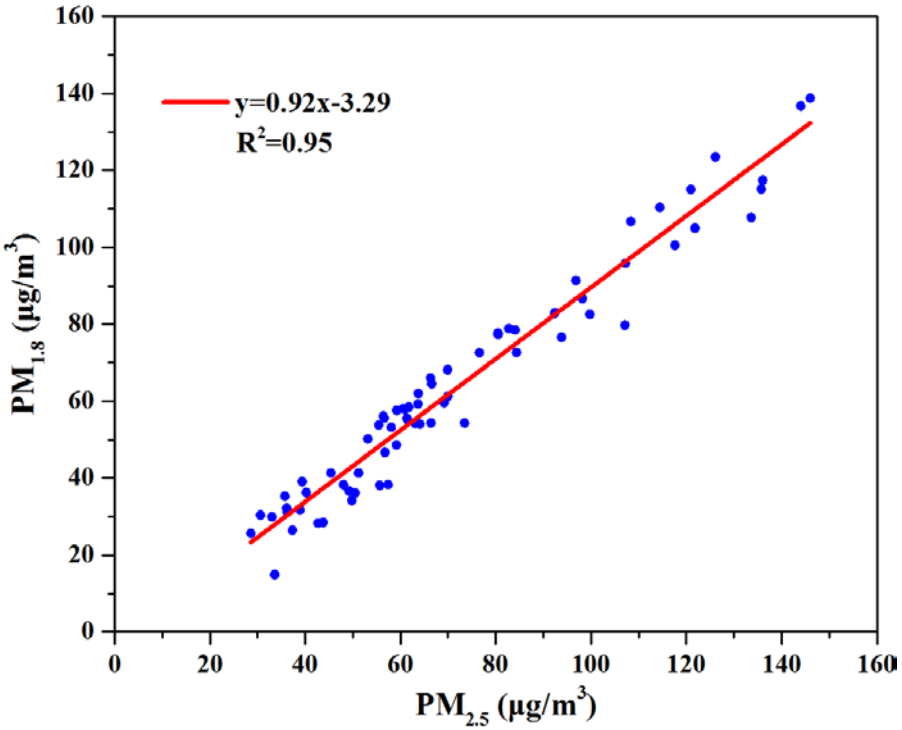

Figure S3. Correlation between the mass concentrations of $PM_{1.8}$ collected with MOUDI impactor and $PM_{2.5}$ collected with TH-150C sampler at NJU.

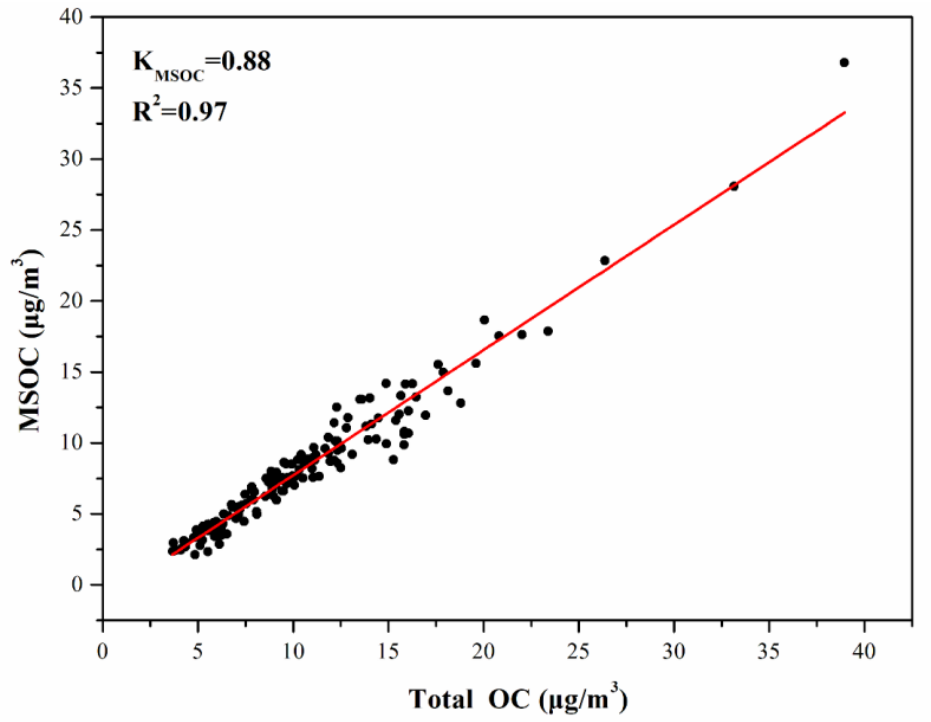

Figure S4. Correlation between MSOC and total OC for all the samples collected in this work. The red line indicates linear regression result with K as slope (intercept is set at zero).

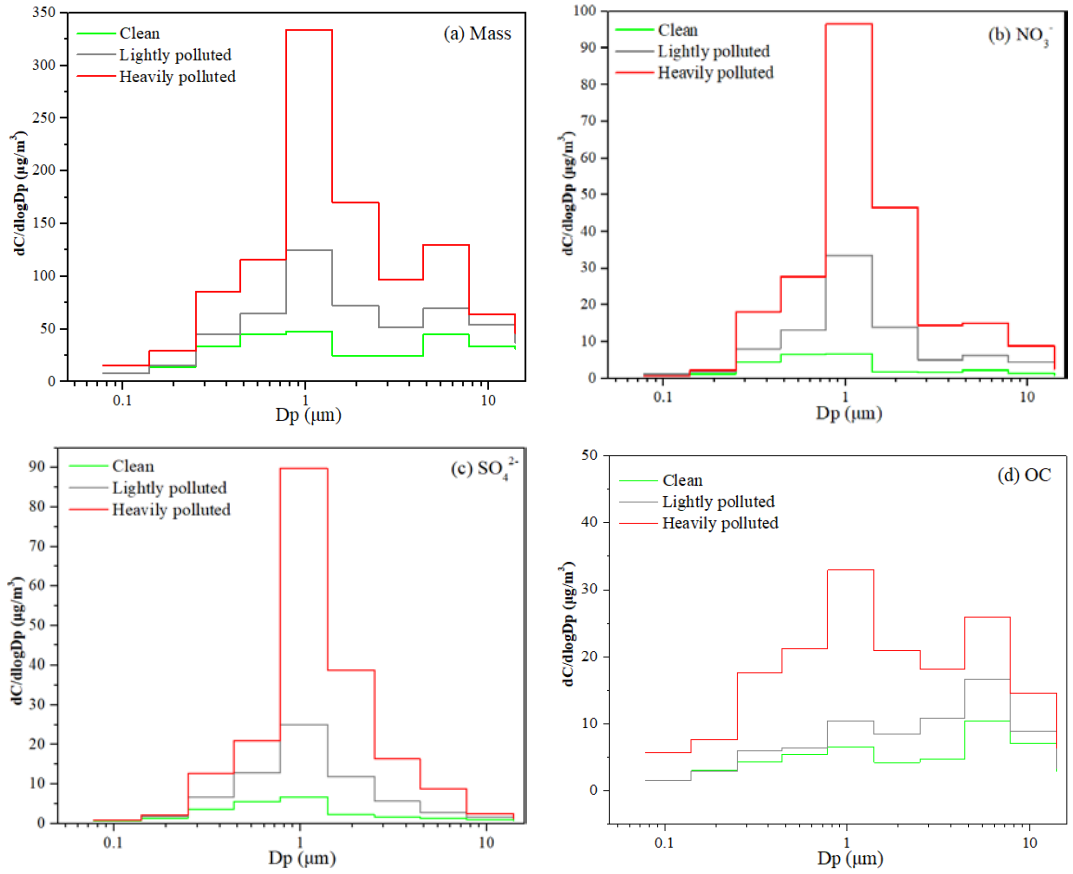

Figure S5. The size distribution of mass concentrations of particles and their main chemical components for the three pollution level periods.

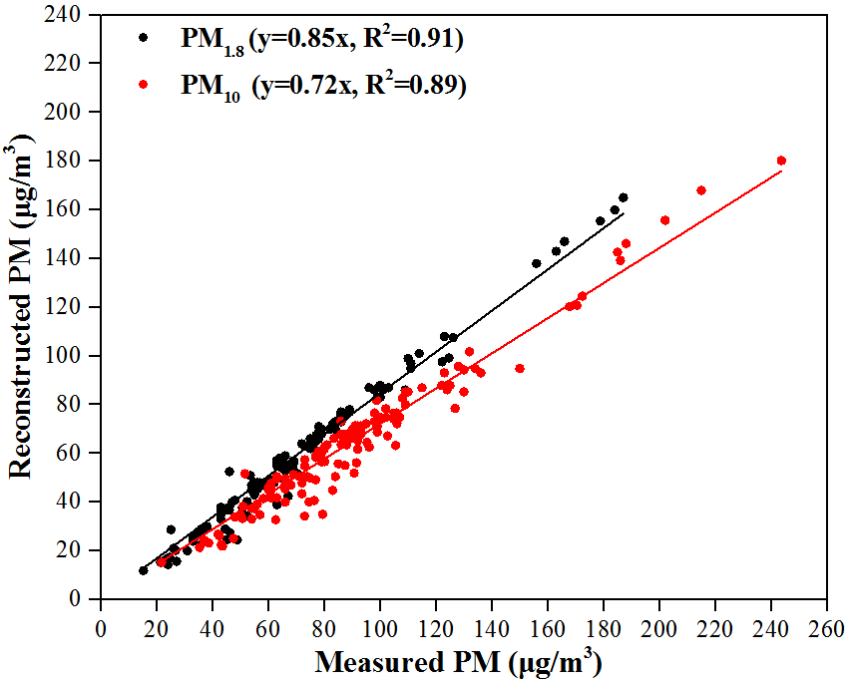

Figure S6. The relationship between the reconstructed and measured PM mass concentrations at the three sites.

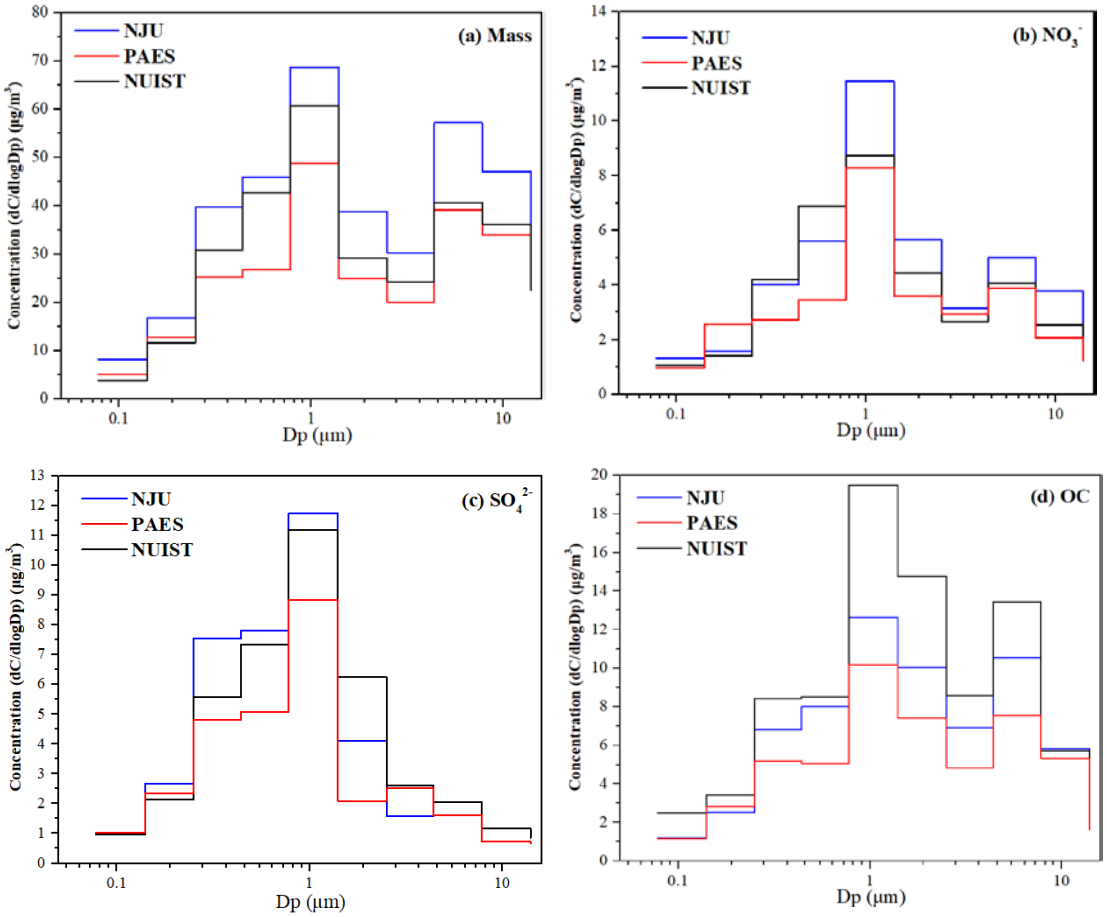

Figure S7. The size distribution of mass concentrations of particles and their main chemical components at NJU, PAES and NUIST.

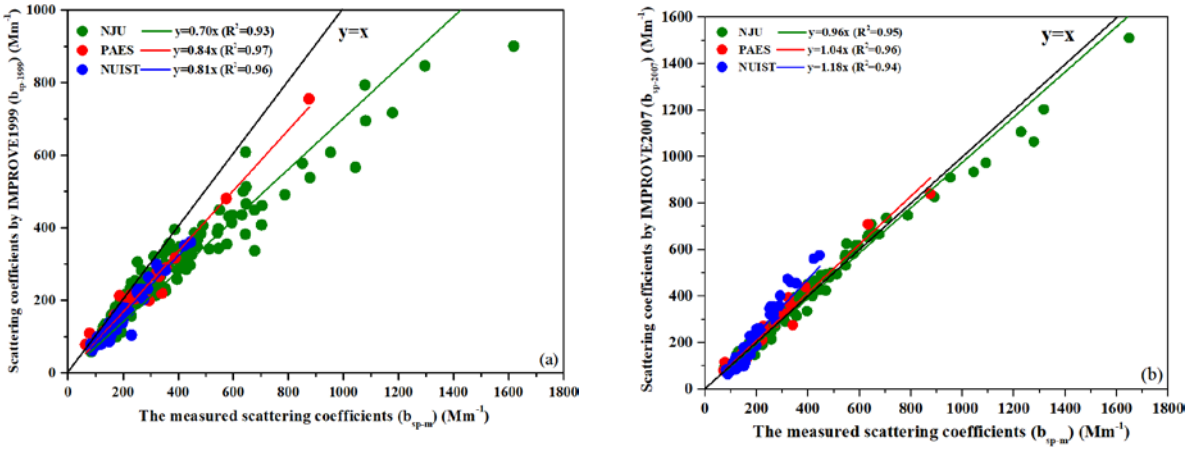

Figure S8. Linear regressions between the measured daily scattering coefficients and those calculated with the IMPROVE1999 algorithm (a) and the IMPROVE2007 algorithm (b) at the three sites.

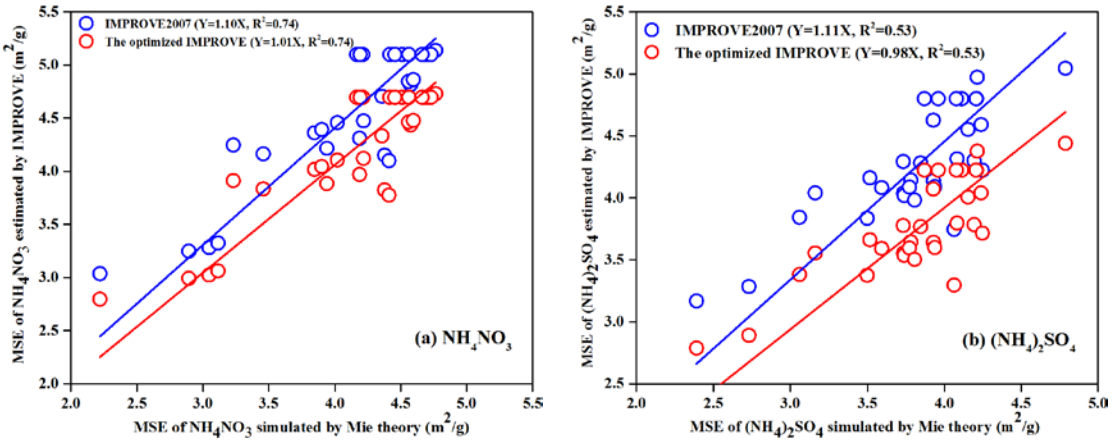

Figure S9. Linear regressions between the mass scattering efficiencies (MSE) of NH_4NO_3 (a) and $(NH_4)_2SO_4$ (b) estimated with the Mie theory and those with the two version of US IMPROVE algorithms.

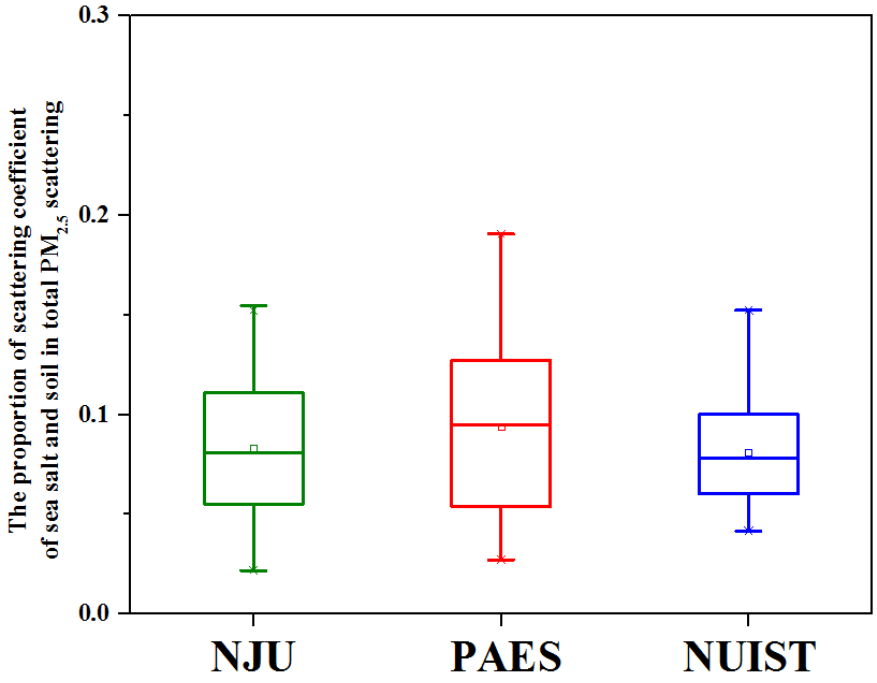

Figure S10 The collective proportions of sea salt and soil dust to the total $PM_{2.5}$ scattering coefficient at the three sites based on the IMPROVE2007 algorithm.

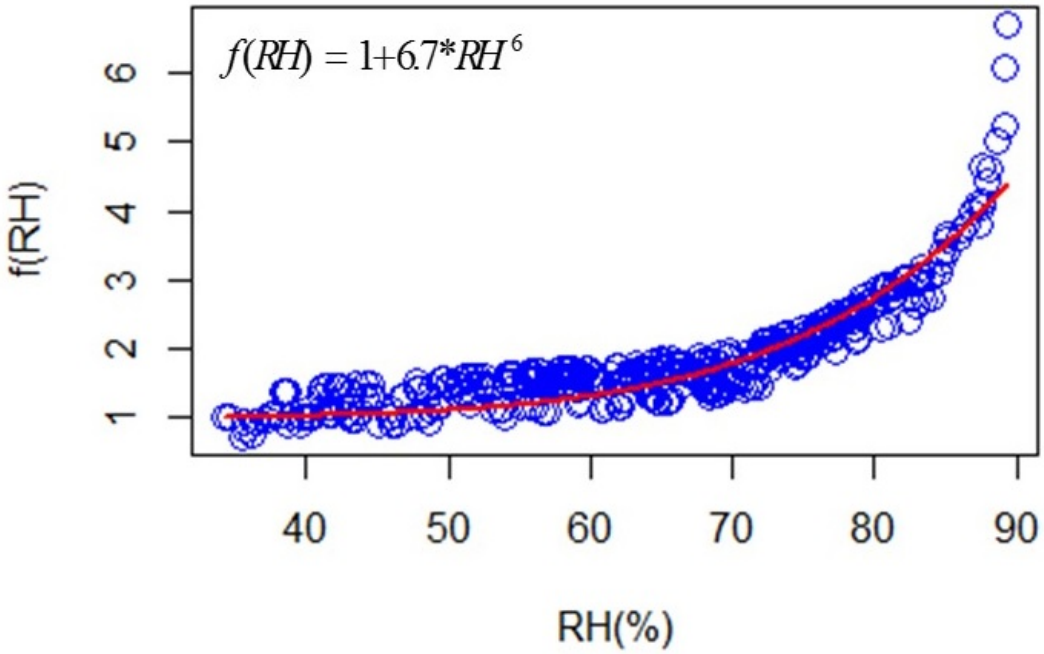

Figure S11. Scattering hygroscopic growth curve of $PM_{2.5}$ at NJU.

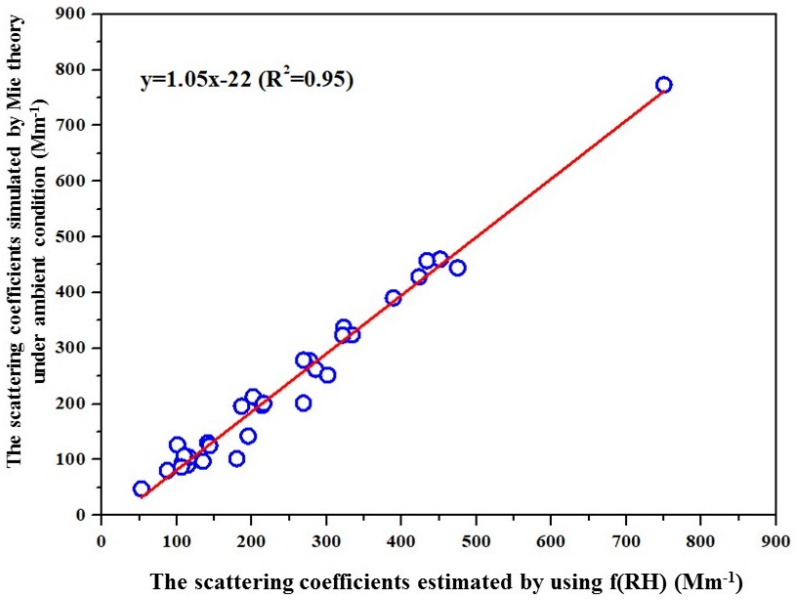

Figure S12. The correlation between the scattering coefficients estimated by f(RH) and those simulated with Mie theory under the ambient conditions.

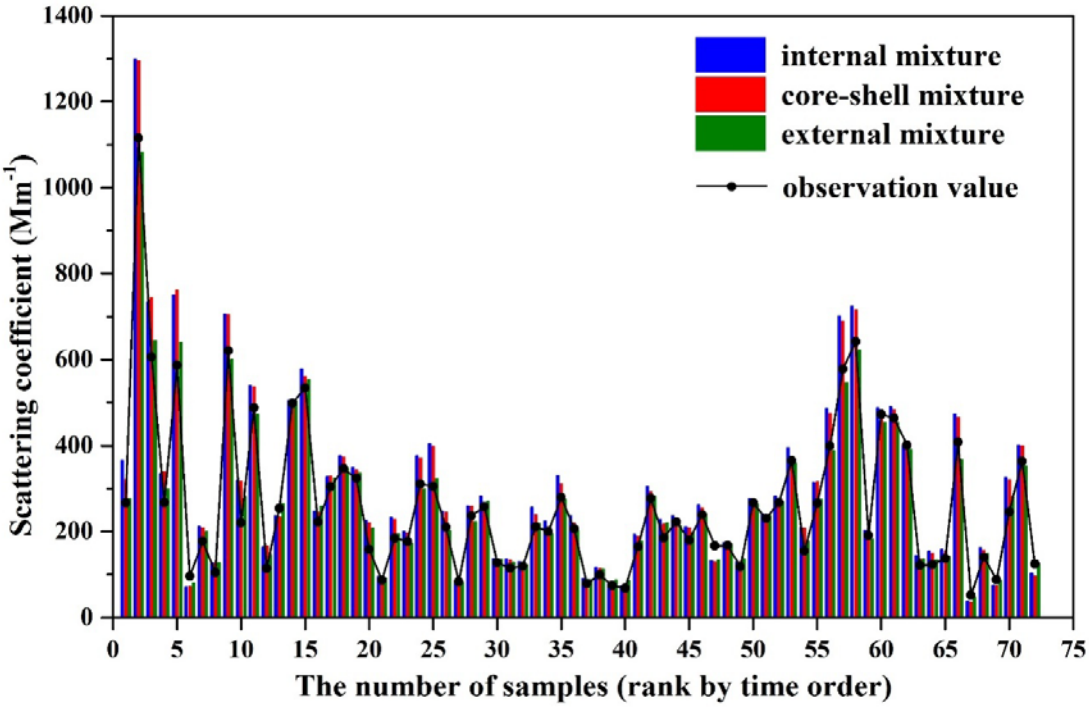

Figure S13. The comparison of the observed scattering coefficients and those estimated with the external, internal, core-shell mixture assumption under the ambient condition at NJU.

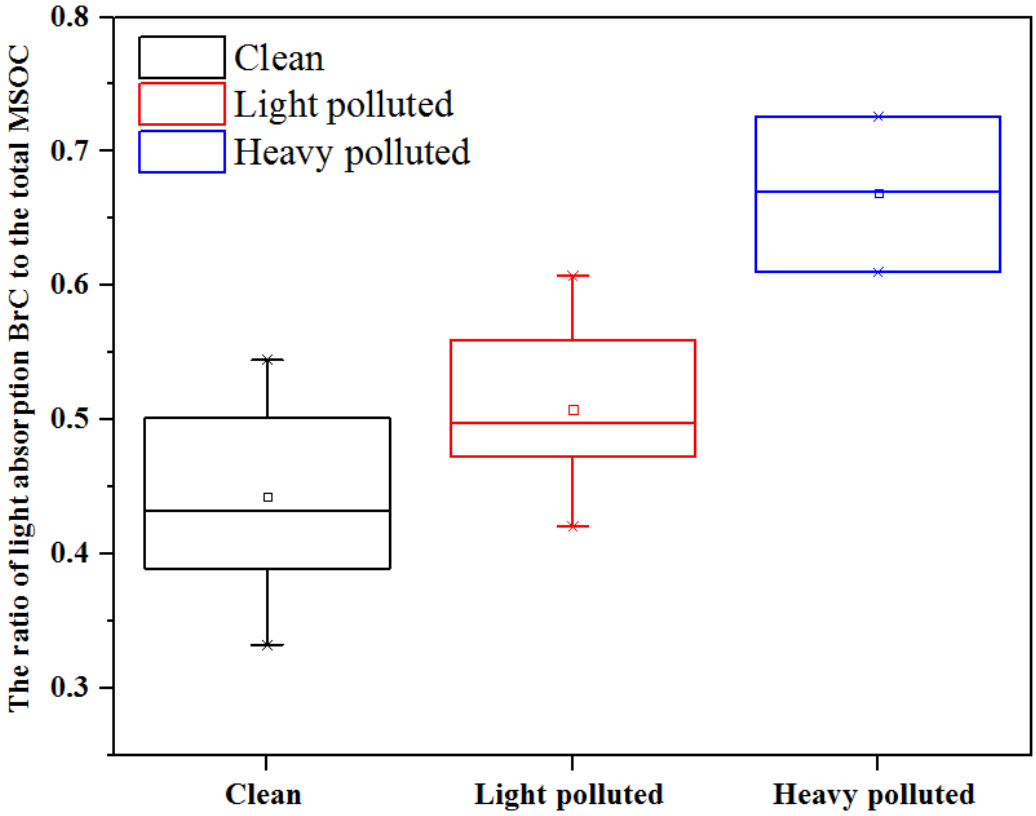

Figure S14. The box plots of the ratios of light absorption BrC mass to the total BrC mass under the three pollution levels. The box plots indicate the mean concentration (square symbols) and the maximum, 99th, 75th, 50th, 25th, 1st percentiles, and minimum.

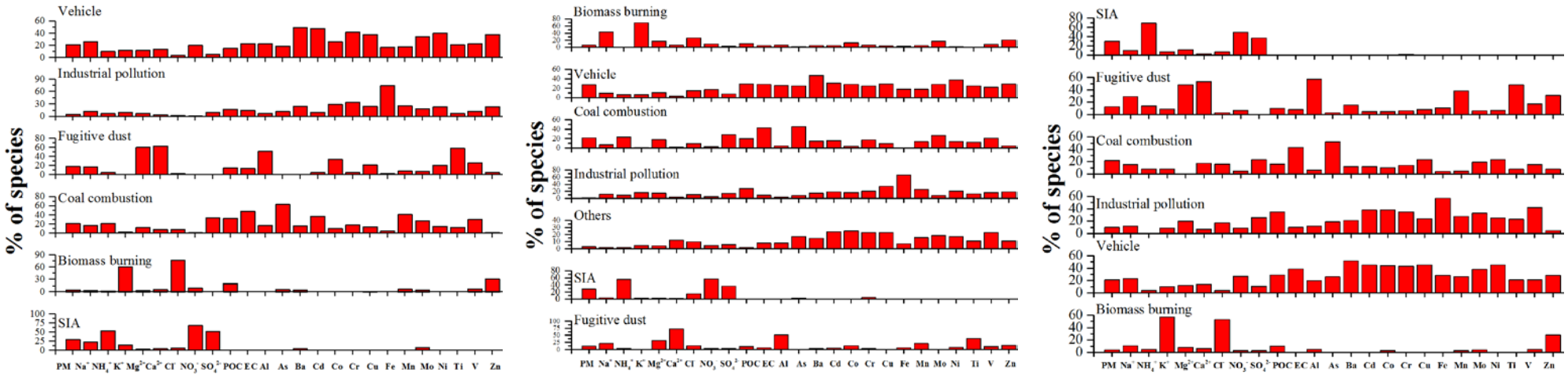

(a) **(b)** **(c)**

Figure S15. The source profiles for accumulation mode particles from the PMF model at NJU (a), PAES (b) and NUIST (c).

REFERENCES

Li, Q., Yin, Y., Gu, X. S., Yuan, L., Kong, S. F., Jiang, Q., Chen, K., Li, L.: An observational study of aerosol hygroscopic growth factor and cloud condensation nuclei in Nanjing in summer, China Environ. Sci., 35, 337-346, 2015.

Pitchford, M., Malm, W., Schichtel, B., Kumar, N., Lowenthal, D., Hand, J.: Revised algorithm for estimating light extinction from IMPROVE particle speciation data, J. Air Waste Manag. Assoc., 57, 1326-1336, doi:10.3155/1047-3289.57.11.1326, 2007.

Wu, Y. X.: Observations of aerosol hygroscopic properties-Case study results over Mt. Huang and Nanjing, MA thesis, Nanjing University of Information Science & Technology, 2014.

Xu, B., Zhang, Z. F., Li, Y. W., Qin, X., Miu, Q., Shen, Y.: Hygroscopic properties of aerosol particles in north suburb of Nanjing in spring. Environ. Sci., 36, 1911-1918, doi:10.13227/j.hjkx.2015.06.001, 2015.

Yu, X. N., Ma, J., Zhu, B., Wang, H. L., Yan, S. Q., Xia, H.: Effects of Relative Humidity and Aerosol Physicochemical Properties on Atmospheric Visibility in Northern Suburb of Nanjing, Environ. Sci., 36, 1919-1925, 2015.

Zhang, J., Wang, L., Chen, J. M., Feng, S. M., Shen, J. D., Jiao, L.: Hygroscopicity of ambient submicron particles in urban Hangzhou, China, Fron. of Environ. Sci. & Engin. in China, 5, 342-347, 2011.